Automated large volume sample preparation for vEM

Erin S. Stempinski[a], Lucas Pagano[b], Jessica L. Riesterer[a,b], Steven K. Adamou[a], Guillaume Thibault[b,c], Xubo Song[b], Young Hwan Chang[c], and Claudia S. López[a,c,d,*]

[a]*Multiscale Microscopy Core, Oregon Health & Science University, Portland, OR, United States*

[b]*Knight Cancer Institute-CEDAR, Oregan Health & Science University, Portland, OR, United States*

[c]*Department of Biomedical Engineering, Oregon Health & Science University, Portland, OR, United States*

[d]*Pacific Northwest Center for Cryo-EM, Oregon Health & Science University, Portland, OR, United States*

**Corresponding author: e-mail address: lopezcl@ohsu.edu*

Chapter outline

Methods in Cell Biology, ISSN 0091-679X, https://doi.org/10.1016/bs.mcb.2023.01.009

Abstract

New developments in electron microscopy technology, improved efficiency of detectors, and artificial intelligence applications for data analysis over the past decade have increased the use of volume electron microscopy (vEM) in the life sciences field. Moreover, sample preparation methods are continuously being modified by investigators to improve final sample quality, increase electron density, combine imaging technologies, and minimize the introduction of artifacts into specimens under study. There are a variety of conventional bench protocols that a researcher can utilize, though most of these protocols require several days. In this work, we describe the utilization of an automated specimen processor, the mPrep™ ASP-2000™, to prepare samples for vEM that are compatible with focused ion beam scanning electron microscopy (FIB-SEM), serial block face scanning electron microscopy (SBF-SEM), and array tomography (AT). The protocols described here aimed for methods that are completed in a much shorter period of time while minimizing the exposure of the operator to hazardous and toxic chemicals and improving the reproducibility of the specimens' heavy metal staining, all without compromising the quality of the data acquired using backscattered electrons during SEM imaging. As a control, we have included a widely used sample bench protocol and have utilized it as a comparator for image quality analysis, both qualitatively and using image quality analysis metrics.

1 Introduction

Biological volume electron microscopy (vEM) was originally developed in response to studying and analyzing comprehensive maps of nervous system connections, also known as connectomics (Peddie et al., 2022; Peddie & Collinson, 2014). However, vEM has become increasingly necessary to further 3D understanding in multiple

research fields, from subcellular components to whole tissues (Guérin, Kremer, Borghgraef, Shih, & Lippens, 2019; Kizilyaprak, Stierhof, & Humbel, 2019; Kremer et al., 2015; Lopez et al., 2018; Midgett, López, David, Maloyan, & Rugonyi, 2017; Peddie et al., 2022; Peddie & Collinson, 2014; Riesterer et al., 2020; Rykiel et al., 2020).

Ideally, vEM protocols used in electron microscopy facilities will be general protocols applicable to numerous specimens and can be used for complementary techniques such as serial block face scanning electron microscopy (SBF-SEM), focused ion beam scanning electron microscopy (FIB-SEM), and array tomography (AT). SBF-SEM provides large volume and field-of-view information at a moderate resolution (in general, 5–15 nm lateral resolution and 30–70 nm in depth), but requires heavy staining to ensure conductivity to prevent charging and obtain good contrast to generate high quality images (Peddie et al., 2022). FIB-SEM, on the other hand, provides higher spatial resolution (4 nm/voxel) in a smaller field of view ideal for a more comprehensive characterization of cellular features and requires less staining to generate good contrast (Peddie et al., 2022). AT simply requires the use of an SEM. Section thickness typically varies between 70 and 100 nm but can be as thin as 40 nm (Wacker & Schroeder, 2013). Lateral resolution depends on the specific imaging modality used. AT can be used in combination with FIB-SEM, where sections are used to rapidly screen large volumes for final milling and imaging of small areas with FIB-SEM (Peddie et al., 2022).

Early vEM protocols used a strategy of osmium tetroxide combined with thiocarbohydrazide to successfully enhance specimen staining (Tapia et al., 2012). With the development of the SBF-SEM, common protocols followed a similar staining regimen of reduced osmium tetroxide, thiocarbohydrazide (TCH), osmium tetroxide, uranyl acetate (UA), and lead aspartate (Deerinck, Bushong, Thor, & Ellisman, 2010; Hua, Laserstein, & Helmstaedter, 2015; Mikula, Binding, & Denk, 2012). Further refinements of these protocols for large samples, such as whole mouse brains, include the use of periodic acid, addition of formamide to the reduced osmium tetroxide step, and substitution of pyrogallol for TCH (Mikula et al., 2012; Mikula & Denk, 2015).

We have used the large-volume protocol developed by Hua et al. (2015) for both SBF- and FIB-SEM, which maintains homogenous, high-contrast staining throughout the specimens in study. This protocol has three main alterations compared to other vEM protocols to achieve this homogenous, high-contrast staining: (a) separating osmium tetroxide and potassium ferrocyanide staining steps instead of combining them, (b) not rinsing between the osmium tetroxide and potassium ferrocyanide steps, and (c) heating the UA solution. However, this protocol, like others referenced here, requires at least 3 days of laborious and time-consuming processing at a fume hood and the handling of hazardous chemicals by the operator prior to the resin polymerization steps. Furthermore, these referenced protocols were established, and therefore optimized, for brain tissue samples. Other laboratories, including ours, have refined this protocol to decrease the amount of time samples are exposed to stains and/or include the use of UA mixed with a percentage of ethanol instead of aqueous UA (Riesterer et al., 2020; Thomas et al., 2021).

Previous literature has also employed the use of a programmable microwave to reduce the amount of time vEM protocols require (Guérin, Kremer, Borghgraef, & Lippens, 2019; Kremer et al., 2015; Lippens, Kremer, Borghgraef, & Guérin, 2019). Steps programmed into this microwave can control factors such as the wattage, whether the magnetron is on or off, and pumping of a vacuum chamber. Staining time has been reduced from over 1 day to about 2 h in total. In these protocols dehydration and infiltration with resin are often performed overnight on the bench, increasing the amount of time that the protocols require (Guérin, Kremer, Borghgraef, & Lippens, 2019; Lippens et al., 2019; Tapia et al., 2012).

Another machine that promises to speed up electron microscopy protocols is an automatic liquid handling processor, the mPrep™ ASP-2000™ automated specimen processor (Microscopy Innovations LLC). The first reference to using an automated specimen processor by Microscopy Innovations for vEM was work performed by McClain, Nowotarski, Zhao, and Alvarado (2017), who used the mPrep™ ASP-1000™, an early model prior to the development of the temperature control module, to process planarian flatworms for array tomography (AT) by following the protocol developed by Deerinck et al. (2010). Since then, the ASP-2000 has been used to process brain tissue, cardiac muscle, and zebrafish larvae for SBF-SEM (Benson, Kidd, Campbell, & Goodman, 2020; Goodman et al., 2019; McClain, Harwood, & Nowotarski, 2019; Peloggia et al., 2021). Others have also heated the UA to enhance staining (McClain et al., 2019) as suggested by Hua et al. (2015), though to our knowledge none have separated the potassium ferrocyanide and osmium tetroxide steps.

In this chapter, we will describe our attempts to translate the protocol by Hua et al. (2015) to the ASP-2000 as well as compare samples processed manually at the bench to those processed by automation. One of the goals of the methods described here is to reduce the amount of operator's time required for sample processing without compromising the staining quality of the specimens. Another goal is to be able to utilize these methods on a wider range of samples typically received at imaging facilities. We also further refine one of the automatic processor protocols to enhance membrane contrast by decreasing staining times and substituting aqueous UA with ethanolic UA. Since not all specimens behave in the same way during sample preparation, we decided to use two different chemically fixed samples in our tests: 100 μm vibratome sections of marmoset brain and pieces of breast cancer tumor from a mouse-derived syngeneic transplant model.

For our study, specimens processed using the automated processor were successfully imaged utilizing both FIB-SEM and SBF-SEM imaging modalities. We aimed to replicate conditions previously used to generate 2D large maps and 3D volumes in bench-processed specimens (Ishibashi et al., 2022; Johnson et al., 2022; Lopez et al., 2018; Midgett et al., 2017; Riesterer et al., 2020; Rykiel et al., 2020). Furthermore, we describe deep learning-based methods used for image quality (IQ) analysis of collected tilesets as an attempt to eliminate human bias during quality assessment.

2 Materials and methods

2.1 ASP-2000

2.1.1 Anatomy of the ASP-2000 automated specimen processor

The ASP-2000 automated specimen processor (Fig. 1A) is equipped with an eight-channel pipette head, allowing for eight samples to be processed simultaneously in a container called an mPrep/s™ capsule (Fig. 1B). The bottom of the mPrep/s capsule is a fine mesh designed to contain the sample while allowing aspiration and dispensation of fluid during the sample preparation procedure (Fig. 1B). The base of the ASP-2000 allows for up to six plates of chemicals and water to be loaded into the automated specimen processor (Fig. 1C). These plates come in two form factors; a plate with 12 vertical channels where the samples will all be exposed to the same solution, and a plate with 96 wells where each sample can be exposed to individual solutions (Fig. 1D). Two of the plates are set above a thermal control unit, which allows for heating of solutions during some processing steps (Fig. 1C). Moreover, each of the two plates can be set to a different temperature. In addition, this unit is equipped with an integrated fume enclosure for venting toxic vapors safely into a fume hood.

Every step of the protocol for the specimen processor is programmable via the user interface (Fig. 1E), with the most often used items being location of the multi-channel pipettor within the ASP-2000, the speed (based on viscosity) at which fluid is aspirated into and dispensed from the mPrep capsules, holding times during the aspiration and dispensing steps, and number of repetitions of the aspiration and dispensing steps. Pauses and notifications can also be programmed into each protocol to allow for filling of fluids in plates, switching plates, insertion or removal of capsules, or other uses. In addition, macros can be programmed into the protocol for specific functions. For example, a "BlowOut" function will expel all the fluids retained within the mPrep/s™ capsule before the next step in our protocols.

2.1.2 Set up the ASP-2000 automated specimen processor

(1) Via the user interface (Fig. 1E) select a pre-loaded protocol. The user can also easily modify a saved protocol to create a new one

(2) Open the temperature control units on the dashboard or the stand-alone program. Ensure the temperature for both controllers is set to 60 °C and the controllers are actively heating (Fig. 1F)

(3) For plates 1, 3, 4, and 6, load the plates into the base of the processor and place the freshly prepared reagents into the respective columns. For plate 2, ensure the fluids are placed in the plate under a fume hood, and seal the plate with a piece of heat-seal foil using the iron. Ensure the foil is tightly secured to the plate before loading it into the ASP-2000. The acetone and resin in plate 5 will be loaded shortly before use. Recipes and solutions utilized can be found in Section 2.4.1

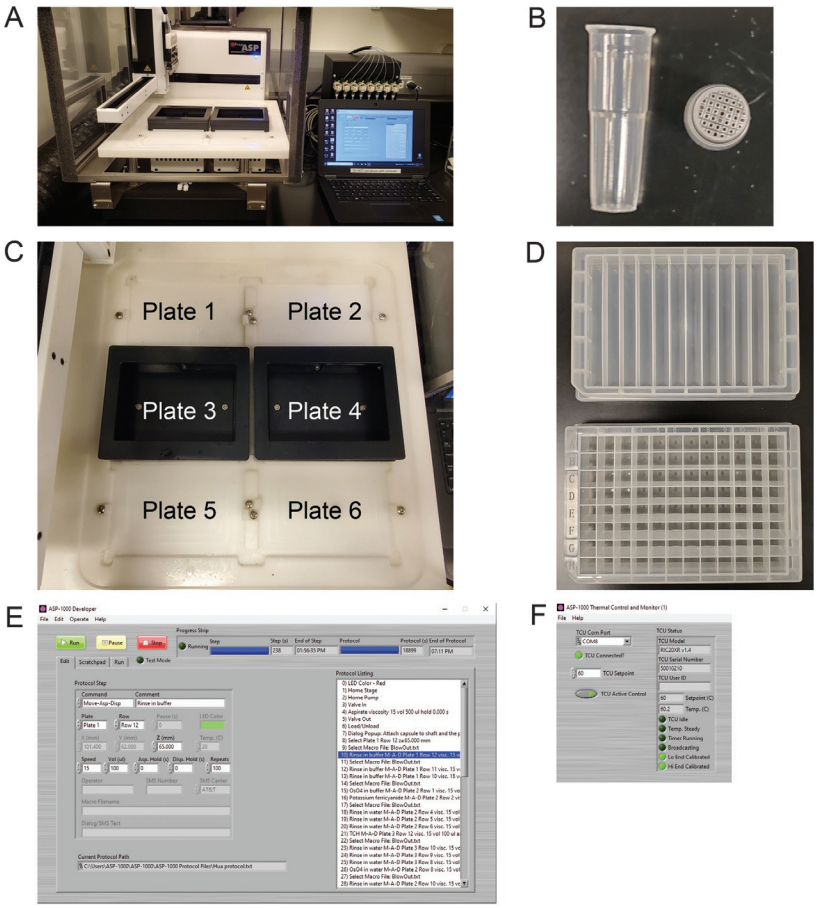

FIG. 1

(A) The mPrep™ ASP-2000™ automated specimen processor. (B) The side and bottom of an mPrep/s™ capsule. (C) The base of the ASP-2000 holds 6 plates, with plates 3 and 4 controlled by a thermal control unit to allow for varying temperatures. (D) Plates come in two form factors; the 12-column plate (top), 96-well plate (bottom). (E) The ASP software allows for programming of each step. (F) Temperature is controlled by the thermal control unit interface.

(4) Under 0.1 M cacodylate buffer, chop tissue into 1 mm^3 pieces using a guillotine-like motion. Place the tissue into buffer-filled mPrep capsules. Attach the mPrep capsules to the pipette head and make sure they are well seated. Remove excess fluid from the capsules with a tissue or paper towel

(5) Press **START** on the UI to initialize the automated processing

Note: Please go to Section 4 of the chapter for more detailed protocol information.

(6) While the samples are in the uranyl acetate plate or lead aspartate plate, load the acetone and resin solutions in plate 5. Cover the plate with a self-adhesive foil seal sheet and place the plate in the ASP-2000
(7) After the sample preparation protocol is finalized, remove the capsules from the pipette head
(8) Polymerization of the resin can be done while the specimens are in the mPrep/s capsules or they can be removed and placed in regular coffin molds. Samples can also be directly mounted on stubs as described by Schieber et al. (2017)

Note: If the orientation of the specimens is important for the research goals, screens can be used to hold the sample in place in the mPrep/s capsule.

2.2 Tissue harvest

2.2.1 Marmosets brains

(1) Marmosets were deeply anesthetized and ventilated. They were then perfused with warmed (37 °C), oxygenated Krebs-Ringer Carbicarb (KRC) buffer for 3 s, and then with 2% formaldehyde and 2.5% glutaraldehyde in 0.1 M cacodylate buffer (pH 7.4)
(2) After 1 h of perfusion, the brain was harvested, postfixed in the same fixation solution at 4 °C for 48 h and sectioned in a vibratome at 100 μm thickness
(3) Sections were stored at −20 °C in cryoprotectant (3% ethylene glycol, 3% glycerol, 0.02 M phosphate buffer) until use for vEM preparation
(4) To remove the cryoprotectant, the specimens were kept at 4 °C and washed in 0.1 M phosphate buffer pH 7.4, with buffer exchanges every 12 h for 3 days immediately leading up to the vEM preparation day
(5) Processing then proceeded according to the protocols described below

Note: All the experiments involving marmosets were conducted in compliance with the Institutional Animal Care and Use Committee of the Salk Institute for Biological Studies and conformed to NIH guidelines.

2.2.2 Mouse-derived syngeneic transplants

Mouse-derived syngeneic transplants (MDSTs) were used as a murine model of breast cancer.

(1) Mouse breast tumor grafts were implanted into the 4th mammary gland of FVB mice
(2) The mice were euthanized using a CO_2 chamber followed by cervical dislocation when tumor volume reached 2 cm
(3) A small piece of tumor tissue was excised from the animal and immediately placed in a tube on ice containing 2.5% glutaraldehyde and 2.5% formaldehyde in 0.1 M sodium cacodylate buffer, pH 7.4
(4) Specimens were stored at 4 °C until use for vEM preparation

Note: All manipulations were approved by Oregon Health & Science University's Institutional Animal Care and Use Committee (IACUC).

2.3 Conventional bench processing

Solutions needed (all prepared fresh):

Buffer: 0.1 M sodium cacodylate buffer (pH 7.4)
2% osmium tetroxide prepared in 0.1 M sodium cacodylate
2% osmium tetroxide prepared in water
2.5% *w/v* ferricyanide in 0.1 M sodium cacodylate
TCH: 1% w/v thiocarbohydrazide in water
Uranyl Acetate: 1% w/v uranyl acetate in water
Embed 812 resin: add 22.36 g EMBed 812, 12.47 g DDSA, 11.93 g NMA together and mix gently to prevent bubbles. Add 0.65 mL BDMA and stir for 30 min. After stirring, apply vacuum for 30 min to remove any air bubbles.

(1) Fixed tumor samples were chopped into approximately 1 mm^3 pieces and fixed brain samples were chopped into $1 \times 1 \times 0.1$ mm pieces and processed according to Hua et al. (2015) with slight modifications (Riesterer et al., 2020)
(2) Day 1: rinse the samples in 0.1 M sodium cacodylate buffer (pH 7.4) five times for 5 min each at room temperature
(3) Immerse the samples in 2% osmium tetroxide prepared in 0.1 M sodium cacodylate and incubate for 90 min at room temperature
(4) Incubate the samples with freshly prepared 2.5% w/v ferricyanide in 0.1 M sodium cacodylate and incubate them for 90 min at room temperature.
(5) Wash specimens five times in water
(6) Incubate the specimens in 1% w/v thiocarbohydrazide (TCH) at 40 °C for 45 min, followed by five rinses in water (5 min per rinse)
(7) Incubate samples with 2% *v*/v aqueous osmium tetroxide for 90 min at room temperature
(8) Rinse tissues five times in water, and incubate them in 1% w/v aqueous UA overnight at 4 °C
(9) Day 2: samples are placed in a 50 °C oven for 2 h and later rinsed five times in water
(10) Specimens are then stained in lead aspartate solution (Hua et al., 2015) at 50 °C for 2 h and rinsed five times in water
(11) Prepare fresh acetone: water series (50%, 75%, 85%, 95%, 100% *v*/v) and incubate the specimens twice for each step for 5 min at room temperature with gentle agitation
(12) Prepare the EMbed 812 resin
(13) Incubate the specimens in a 1:1 EMbed 812 resin: acetone mix for 40 min at room temperature with gentle agitation
(14) Incubate the specimens in a 3:1 Embed 812 resin:acetone mix for 40 min at room temperature with gentle agitation
(15) Infiltrate the sample overnight with pure resin at room temperature with gentle agitation

(16) Day3: samples are exchanged in pure resin four times for 30 min each with gentle agitation
(17) Polymerize the samples in EM molds in a 60 °C oven for 48 h
(18) Day5: samples can be removed from the oven and trimmed for image acquisition

2.4 Automated processing for vEM

(1) Fixed brain specimens are chopped into $1 \times 1 \times 0.1$ mm samples and fixed tumor specimens are chopped into approximately 1 mm^3 using razor blades under 0.1 M sodium cacodylate buffer
(2) Place the mPrep/s capsules in the mPrep/Bench rack and fill with one or two drops of 0.1 M sodium cacodylate buffer. Place at least one piece of tissue per mPrep/s capsule. Up to 8 capsules can be loaded per processing session

Note: Up to four pieces of tissue can be incubated within the same capsule without compromising staining quality.

(3) Load the plates with the solutions needed for the processing as indicated in Fig. 2
(4) Mount the plates on the specimen processor's base (Fig. 1C)
(5) Load the protocol to be utilized on the ASP-2000 user interface and start the procedure
(6) The protocols utilized here are as follows:

Note: Several functions of the ASP-2000 automated processor can be modified to optimize sample preparation such as:

(a) viscosity rate: "visc" this value sets the peristaltic pump speed. Values range from 0 to 40, where 40 is the slowest. In our case, the default value is 15
(b) volume: "vol" in μL, this value sets the default volume of the reagent to be aspirated or dispensed
(c) aspirate: "asp" in seconds, this value sets the default hold time after the aspiration has been completed
(d) dispense: "disp" in seconds, this value sets the default wait time after dispensing has been completed
(e) repetitions: "rpt" this value sets the default number of times in which the reagent is aspirated and dispensed during a step

2.4.1 ASP-2000 aqueous uranyl acetate

Solutions needed (all prepared fresh):

Buffer: 0.1 M sodium cacodylate buffer (pH 7.4)
OsO4: 2% osmium tetroxide prepared in 0.1 M sodium cacodylate
Potassium ferricyanide: 2.5% w/v ferricyanide in 0.1 M sodium cacodylate
TCH: 1% w/v thiocarbohydrazide in water
Uranyl Acetate: 1% w/v in water
Resin: follow recipe from Section 4 of this chapter.

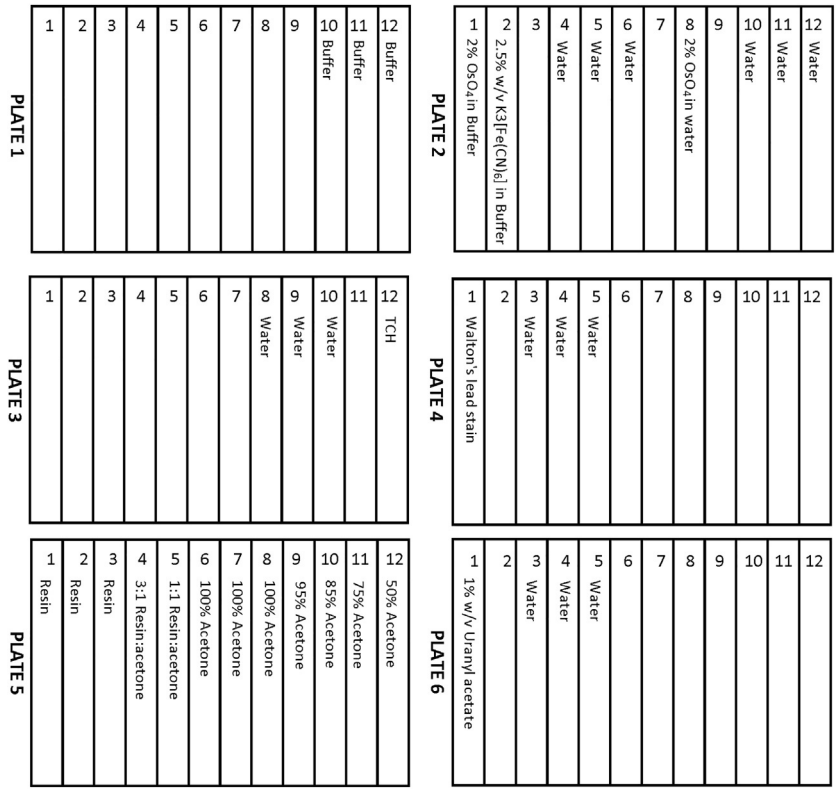

FIG. 2

Plate map showing the reagents required to be loaded prior using the protocols described here. Buffer: 0.1 M sodium cacodylate buffer (pH 7.4), TCH: 1% *w/v* Thiocarbohydrazide in water.

Walton's lead: as described in Hua et al. (2015)

(0) Home Stage
(1) Home Pump
(2) Valve In
(3) Aspirate viscosity 15 vol 500 µL hold 0.000 s
(4) Valve Out
(5) Load/Unload
(6) Dialog Popup: Attach capsule to shaft and the press "Enter".
(7) Select Plate 1 Row 12 z = 65.000 mm
(8) Select Macro File: BlowOut.txt
(9) Rinse in buffer M-A-D Plate 1 Row 12 vise. 15 vol 100 µL asp 0.000 s disp 0.000 s rpt 100
(10) Select Macro File: BlowOut.txt

(11) Rinse in buffer M-A-D Plate 1 Row 11 vise. 15 vol 100 µL asp 0.000 s disp 0.000 s rpt 100
(12) Rinse in buffer M-A-D Plate 1 Row 10 vise. 15 vol 100 µL asp 0.000 s disp 0.000 s rpt 100
(13) Select Macro File: BlowOut.txt
(14) OsO4 in buffer M-A-D Plate 2 Row 1 vise. 15 vol 100 µL asp 2.000 s disp 0.000 s rpt 200
(15) Potassium ferricyanide M-A-D Plate 2 Row 2 vise. 15 vol 100 µL asp 2.000 s disp 0.000 s rpt 200
(16) Select Macro File: BlowOut.txt
(17) Rinse in water M-A-D Plate 2 Row 4 vise. 15 vol 100 µL asp 0.000 s disp 0.000 s rpt 100
(18) Rinse in water M-A-D Plate 2 Row 5 vise. 15 vol 100 µL asp 0.000 s disp 0.000 s rpt 100
(19) Rinse in water M-A-D Plate 2 Row 6 vise. 15 vol 100 µL asp 0.000 s disp 0.000 s rpt 100
(20) TCH M-A-D Plate 3 Row 12 vise. 15 vol 100 µL asp 2.000 s disp 0.000 s rpt 200
(21) Select Macro File: BlowOut.txt
(22) Rinse in water M-A-D Plate 3 Row 10 vise. 15 vol 100 µL asp 0.000 s disp 0.000 s rpt 100
(23) Rinse in water M-A-D Plate 3 Row 9 vise. 15 vol 100 µL asp 0.000 s disp 0.000 s rpt 100
(24) Rinse in water M-A-D Plate 3 Row 8 vise. 15 vol 100 µL asp 0.000 s disp 0.000 s rpt 100
(25) OsO4 in water M-A-D Plate 2 Row 8 vise. 15 vol 100 uL asp 2.000 s disp 0.000 s rpt 200
(26) Select Macro File: BlowOut.txt
(27) Rinse in water M-A-D Plate 2 Row 10 vise. 15 vol 100 µL asp 0.000 s disp 0.000 s rpt 100
(28) Rinse in water M-A-D Plate 2 Row 11 vise. 15 vol 100 µL asp 0.000 s disp 0.000 s rpt 100
(29) Rinse in water M-A-D Plate 2 Row 12 vise. 15 vol 100 µL asp 0.000 s disp 0.000 s rpt 100
(30) 1% aqueous Uranyl acetate M-A-D Plate 6 Row 1 vise. 15 vol 100 µL asp 2.000 s disp 0.000 s rpt 200
(31) Select Macro File: BlowOut.txt
(32) Rinse in water M-A-D Plate 6 Row 3 vise. 15 vol 100 µL asp 0.000 s disp 0.000 s rpt 100
(33) Rinse in water M-A-D Plate 6 Row 4 vise. 15 vol 100 µL asp 0.000 s disp 0.000 s rpt 100
(34) Rinse in water M-A-D Plate 6 Row 5 vise. 15 vol 100 µL asp 0.000 s disp 0.000 s rpt 100
(35) Walton's lead M-A-D Plate 4 Row 1 vise. 15 vol 100 µL asp 2.000 s disp 0.000 s rpt 200
(36) Select Macro File: BlowOut.txt

(37) Rinse in water M-A-D Plate 4 Row 3 vise. 15 vol 100 µL asp 0.000 s disp 0.000 s rpt 100
(38) Rinse in water M-A-D Plate 4 Row 4 vise. 15 vol 100 µL asp 0.000 s disp 0.000 s rpt 100
(39) Rinse in water M-A-D Plate 4 Row 5 vise. 15 vol 100 µL asp 0.000 s disp 0.000 s rpt 100
(40) 50% Acetone M-A-D Plate 5 Row 12 vise. 15 vol 100 µL asp 0.000 s disp 0.000 s rpt 100
(41) 75% Acetone M-A-D Plate 5 Row 11 vise. 15 vol 100 µL asp 0.000 s disp 0.000 s rpt 100
(42) 85% Acetone M-A-D Plate 5 Row 10 vise. 15 vol 100 µL asp 0.000 s disp 0.000 s rpt 100
(43) 95% Acetone M-A-D Plate 5 Row 9 vise. 15 vol 100 µL asp 0.000 s disp 0.000 s rpt 100
(44) 100% Acetone M-A-D Plate 5 Row 8 vise. 15 vol 100 µL asp 0.000 s disp 0.000 s rpt 100
(45) 100% Acetone M-A-D Plate 5 Row 7 vise. 15 vol 100 µL asp 0.000 s disp 0.000 s rpt 100
(46) Select Macro File: BlowOut.txt
(47) 100% Acetone M-A-D Plate 5 Row 6 vise. 15 vol 100 µL asp 0.000 s disp 0.000 s rpt 100
(48) 50% Resin M-A-D Plate 5 Row 5 vise. 15 vol 100 µL asp 0.000 s disp 0.000 s rpt 100
(49) 75% Resin M-A-D Plate 5 Row 4 vise. 15 vol 100 µL asp 10.000 s disp 0.000 s rpt 100
(50) 100% Resin M-A-D Plate 5 Row 3 vise. 15 vol 100 µL asp 10.000 s disp 0.000 s rpt 100
(51) 100% Resin M-A-D Plate 5 Row 2 vise. 15 vol 100 µL asp 10.000 s disp 0.000 s rpt 200
(52) 100% Resin M-A-D Plate 5 Row 1 vise. 15 vol 100 µL asp 10.000 s disp 0.000 s rpt 200
(53) Aspirate viscosity 15 vol 100 µL hold 0.000 s
(54) Move capsules up Dialog Popup: Press "Enter" to position capsules for removal
(55) Dispense viscosity 15 vol 100 µL hold 0.000 s
(56) 100% Resin Select Plate 5 Row 1 z = 0.000 mm
(57) Dialog Popup: Capsules ready for removal, press "Enter" to home stage
(58) Home Stage
(59) Home Pump

Note: TCH and lead aspartate staining and rinse steps were performed in plates heated to 60 °C. The uranyl acetate staining was performed at room temperature with no cooling or heating step.

The blowout macro protocol is as follows:
(0) Dispense viscosity 15 vol 100 µL hold 0.000 s
(1) Valve In

(2) Aspirate viscosity 15 vol 100 µL hold 0.000 s
(3) Valve Out

At the end of the protocol, samples were removed from the mPrep/s capsules with a wood stick, placed in an embedding mold with fresh resin, and polymerized in an oven at 60 °C. Specimens can also be polymerized in the mPrep/s capsules if preferred.

2.4.2 ASP-2000 with ethanolic uranyl acetate

This protocol follows the same procedure described in Section 2.4.1 with a modification in step 31, in which the incubations with uranyl acetate are done in 1% *w*/*v* uranyl acetate prepared in 25% *v*/v ethanol.

2.4.3 Fast ASP-2000 with ethanolic acid

This protocol follows the same procedure described in Section 2.4.1 but reduces the number of repetitions from 200 to 100 during staining steps 15, 16, 21, 26, 31, and 36. In addition, a solution of 1% UA in 25% ethanol was used as described in Section 2.4.2.

2.5 Sample mounting and preparation for imaging

Samples recovered after the 36 h polymerization incubation at 60 °C are treated as follows:

2.5.1 Sample mounting for FIB-SEM and SBF-SEM block face imaging

(1) Mount trimmed resin blocks on an aluminum stub for a Thermo Scientific VolumeScope II with H20E EPO-TEK conductive silver epoxy. The two components need to be mixed well at a one-to-one ratio before use
(2) Cure the epoxy resin at 60 °C overnight in a conventional oven
(3) Trim excess resin away using a razor blade and face the sample on an ultramicrotome using a diamond knife
Note: In our case we utilized a Leica UC7 ultramicrotome fitted with a Trim 45 Diatome knife.
(4) Coat the specimens with 8 nm of carbon using a Lecia ACE 600 coater. If additional conductivity is needed, Leitsilber can be applied to the sides of the specimen that are not covered by the EPO-TEK silver resin

Note: The carbon coating described here only applies to samples that will only be analyzed for tissue and staining quality. If the final goal is to study the specimens by SBF-SEM on Thermo Scientific equipment, they need to be coated with 20 nm of gold as described in Riesterer et al. (2020).

2.5.2 Sample mounting for array tomography imaging

(1) Trim the marmoset brain sample processed with the ASP ethanolic UA method with a diamond knife to obtain parallel sides
(2) Apply a 3:1 mixture of xylene: rubber cement glue to the top and bottom of the block face to help the sections adhere as a ribbon

(3) Section the specimen on a Leica UC7 ultramicrotome to obtain ribbons of sections of 100 nm thick
(4) Clean silicon chips using 70% ethanol solution and glow discharge them for 1 min at 15 mA on a PELCO Easiglow glow discharge unit
(5) Place the ribbons of sections on the cleaned silicon chip and air dry the ribbons
(6) Mount the silicon chip on an aluminum stub with a carbon tab

2.6 Block face imaging: Quality control for vEM procedures

For the purpose of this chapter, the samples described here were not submitted to conventional FIB-SEM and SBF-SEM data acquisition. In order to evaluate the quality of the tissues and the staining procedures described here, we only acquired images on the block face of the specimens. For a more detailed methodology to acquire FIB-SEM and SBF-SEM volumes please refer to Riesterer et al. (2020) and Rykiel et al. (2020).

2.6.1 Thermo Fisher Scientific VolumeScope 2 SBF-SEM image acquisition

Samples described here were imaged in a Thermo Scientific VolumeScope 2 SBF-SEM under high vacuum conditions. Images were acquired in VolumeScope mode using the T1 detector with the filter ring installed. Electron beam conditions utilized were 2 keV with a beam current of 200pA at a 3 µs dwell time. All images were acquired at a working distance (WD) of 6.5 mm with 6144 × 4096 pixels tiff images at a horizontal field of width (HFW) of 122, 61.44 and 30.72 µm, respectively. These magnifications represent typical fields-of-view and resolutions acquired during SBF-SEM data collection. Single images as well as tilesets were acquired for image analysis. Tilesets were acquired using the Thermo Scientific Maps™ software package. For brain samples, 8 × 3 tile arrays were mapped with HFW 61.44 µm, while tumor specimens were mapped using the same imaging conditions and a 5 × 5 tile array. Array size and aspect ratio differed due to tissue shape (long and narrow vs bulk).

It is worth mentioning that tilesets collected for the same specimen were all acquired in a single imaging session with no instrument venting. Tilesets submitted for image quality analysis were acquired by the same operator to avoid the introduction of any biased brightness and contrast values due to operator preference. Images in these tilesets had the same brightness and contrast values across all processing protocols for each sample and instrument.

2.6.2 Thermo Fisher Scientific Helios NanoLab G3 FIB-SEM image acquisition

Samples described here were imaged using a FEI Helios NanoLab G3 FIB-SEM. Images were acquired using the dedicated Concentric Backscatter Detector (CBS) with all rings active. Electron beam conditions utilized were 3 keV, 200pA, and 3 µs dwell time. All images were acquired at a WD of 4 mm with 6144 × 4096 pixels tiff images using HFW of 61.4, 30.7 and 15 µm. Tilesets were again acquired using the Thermo Scientific Maps™ software package with the previously-mentioned imaging conditions. While the In-Column Detector (ICD) is our preferred detector

for FIB-SEM vEM dataset collection, this detector creates a circular shadow within images that visualizes the bore of the microscope due to the detector being located high within the e-column. This shadow moves depending on the working distance used and is typically removed using post-processing techniques. We chose to use the CBS in this study to create consistent conditions that would not influence our noise-detection results.

Note: A software patch is available for modern Thermo Scientific FIB-SEM models to allow CBS insertion during FIB-SEM image stack collection.

2.6.3 Thermo Fisher Scientific Helios UC5 array tomography image acquisition

Array tomography imaging was performed in Thermo Scientific Helios 5 UC FIB-SEM equipped with Thermo Scientific Maps™ software package for array tomography. Electron beam conditions utilized were 3 keV, 200pA, and 3 µs dwell time. Images were acquired with the retractable CBS detector with all rings active at a WD of 4 mm, as 6144 × 4096 pixels tiff images using a HFW of 30.7 µm.

2.7 Image quality (IQ) analysis

In an effort to quantify image quality with respect to protocol used, but without introducing human bias via sample visible inspection, computer-aided models to evaluate several image quality metrics were implemented. We tried evaluating the metrics both on entire stitched tilesets and on individual tiles. As results were very similar, we only show the latter here. It is important to note that evaluating the collected images is difficult; as they are not from the same sample, they do not image the same region of interest, and thus their content is dissimilar.

Since a pixel-to-pixel comparison of images is impossible because they do not represent the exact same area of interest, we partially annotated resin in each of them, as can be seen in Fig. 3. As resin is an identical external material added to each sample, this enables noise evaluation by computing the signal's standard deviation in the annotated parts without having to consider signal disparities. Thus, lower values of standard deviation will mean less noise and better IQ. We also use BRISQUE (Blind/Referenceless Image Spatial Quality Evaluator) (Mittal, Moorthy, & Bovik, 2012), which allows the evaluation of IQ without a reference image (ground truth), and yields a score between 0 and 100, where lower values are indicative of better IQ. This method is based on scene statistics of locally normalized luminance coefficients to quantify possible losses of "naturalness" in the image due to the presence of distortions. BRISQUE has been shown to be highly competitive and computationally more efficient than other No-Reference IQ metrics on medical images (Chow & Paramesran, 2016).

Most IQ metrics use a reference image to compare with the degraded image to analyze, but in our case these references do not exist. However, we were able to train a deep learning-based denoising model called Noise2Void to remove the noise from our images without requiring any ground truth (Krull, Buchholz, & Jug, 2019). We

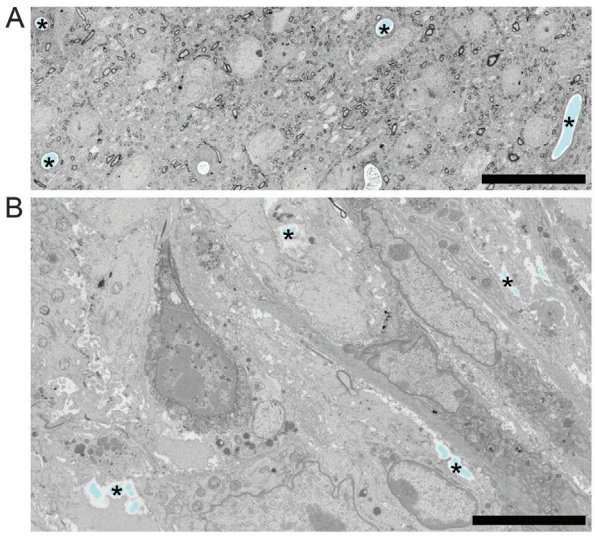

FIG. 3

Examples of hand-annotated resin for noise measurements. Areas annotated are marked by an asterisk and blue coloration. (A) Annotated resin in bench-processed brain imaged with the SBF-SEM. Scale bar = 40 μm. (B) Annotated resin in ASP-2000 mouse tumor imaged with the FIB-SEM. Scale bar = 20 μm.

then used the denoised images as references to their noisy counterparts and compare them using the IQ metrics described below:

- *Peak Signal-to-Noise Ratio (PSNR)* is based on Mean Standard Error and is a point-wise IQ metric. Typical values for PSNR range between 30 and 50 dB, where higher is better. It is frequently used in case studies and benchmarks as a weak evaluator baseline, but it is known to give results far from human perception (Hore & Ziou, 2010)
- *Structural Similarity Index Measure (SSIM)* is based on luminance, contrast and structure, while introducing the concept of inter-dependency between spatially close pixels by being computed on various windows in the image (Hore & Ziou, 2010; Wang, Bovik, Sheikh, & Simoncelli, 2004). Values range from 0 to 1, with 1 being perfect structural similarity
- *Multi-scale Structural Similarity Index Measure (MSSIM)* is a multi-scale version of SSIM which introduces an image synthesis approach that automatically determines the relative importance of each scale (Wang, Simoncelli, & Bovik, 2003). Like SSIM, values range from 0 to 1, with 1 indicating best quality
- *Spectral Residual Based Similarity Index Measure (SR-SIM)* compares the spectral residual saliency maps of the images. SR-SIM is designed on the

hypothesis that an image's saliency map is closely related to its perceived quality (Zhang & Li, 2012). Values range from 0 to 1, with 1 being the best possible score

- *Gradient Magnitude Similarity Deviation (GMSD)* evaluates the difference between the images' gradients. GMSD is based on the pixel-wise gradient magnitude similarity (GMS) and a novel pooling strategy: instead of using the average as is usually done (and works poorly because it ignores the difference in quality degradation relative to each area), the final score is given by the standard deviation of the Gradient Magnitude Similarity map, which is the range of distortions severities between images: the higher the GMSD score, the larger the distortion range, thus the lower the IQ (Xue, Zhang, Mou, & Bovik, 2013). Values range from 0 to 1, where lower is better
- *Deep Image Structure and Texture Similarity (DISTS)* makes use of neural networks to assess IQ. It has been shown to give a closer evaluation of human quality perception than other previously described IQ metrics. In particular, it is less sensitive to point-by-point deviations between the images (Ding, Ma, Wang, & Simoncelli, 2020). Values range from 0 to 1, where 1 is a perfect score

3 Results

3.1 Sample processing time

In our hands, conventional bench processing required 2.5 days prior to embedding with over 5.5 h of active operator time preparing and exchanging solutions. However, the protocols described here using the ASP-2000 automated processor required a total sample preparation time of 7 h prior to embedding with only 2.5 h of active technician time needed. The decrease in staining time for the faster ASP-2000 protocol, as compared to the regular ASP-2000 protocol described here, only reduced the overall processing time by 40 min (Table 1).

3.2 Image contrast comparison

As indicated in Section 2, the same brightness and contrast values across all processing protocols for each sample and imaging modality were utilized to analyze the overall staining quality of the samples. A direct comparison of images acquired for the brain samples processed with the ASP-2000 protocols showed a decrease in overall contrast and signal when compared to the conventional bench protocol analyzed both by FIB-SEM and SBF-SEM detectors (Fig. 4A–H). Using the same detector conditions, we observed that the addition of ethanolic UA in the ASP-2000 protocols increased the contrast of myelin membranes of samples imaged with the FIB-SEM CBS detector (Fig. 4F). However, this was not the case for images acquired with the SBF-SEM (Fig. 4E).

Table 1 A comparison between the bench, ASP-2000, and fast ASP-2000 steps.

	Timing of steps		
Description of steps	**Bench**	**ASP-2000**	**Fast ASP-2000**
Rinse in sodium cacodylate buffer	3 × 5′	3 × 3′	3 × 3′
2% osmium tetroxide in buffer	90′	13′	6.5′
2.5% potassium ferricyanide in buffer	90′	13′	6.5′
Rinse in water	5 × 5′	3 × 3′	3 × 3′
1% thiocarbohydrazide	45′	13′	6.5′
Rinse in water	5 × 5′	3 × 3′	3 × 3′
2% osmium tetroxide in water	90′	13′	6.5′
Rinse in water	5 × 5′	3 × 3′	3 × 3′
1% UA aqueous or 1% UA in 25% EtOH	Overnight +120′	13′	6.5′
Rinse in water	5 × 5′	3 × 3′	3 × 3′
Walton's lead stain	120′	13′	6.5′
Rinse in water	5 × 5′	3 × 3′	3 × 3′
Acetone dehydration *Bench: all steps x2: 50%, 75%, 85%, 95%, 100%* *Automated: 50%, 75%, 85%, 95%, 100% x 3*	50′	21′	21′
Resin infiltration *Bench: Acetone:Resin 1:1, 1:3, Pure resin x5* *Automated: Acetone:Resin 1:1, 1:3, Pure resin x3*	Overnight +200′	123′	123′

A short description of each step is given with the number of minutes and any repetitions. The total time is given in days and/or minutes.

In all cases, the final image brightness and contrast values for both the ASP-2000 protocol with aqueous UA and ethanolic UA, can be rectified with the detector contrast controls (Fig. 5A–H) to give visual results that are similar to those obtained with the bench protocol (Fig. 5A and B). These results indicate that the ASP-2000 methods can be utilized for vEM techniques using the equipment described here.

With these results, we wondered if staining times could be reduced further with the thought that the constant agitation provided by the ASP-2000 could allow for times similar to or faster than those used with microwave preparations from previous literature. We, therefore, decided to reduce the staining times by half for the fast ethanolic UA protocol (Table 1). The brain sample processed with the fast ethanolic UA protocol showed a reduction in contrast of myelinated membranes that was not ameliorated by the addition of ethanolic UA in both imaging platforms (Fig. 4G and H). However, as mentioned above, manipulation of brightness and contrast controls of the detectors were able to compensate for the decrease in staining signal with the FIB-SEM (Fig. 5H). Unfortunately, this was not the case for the same

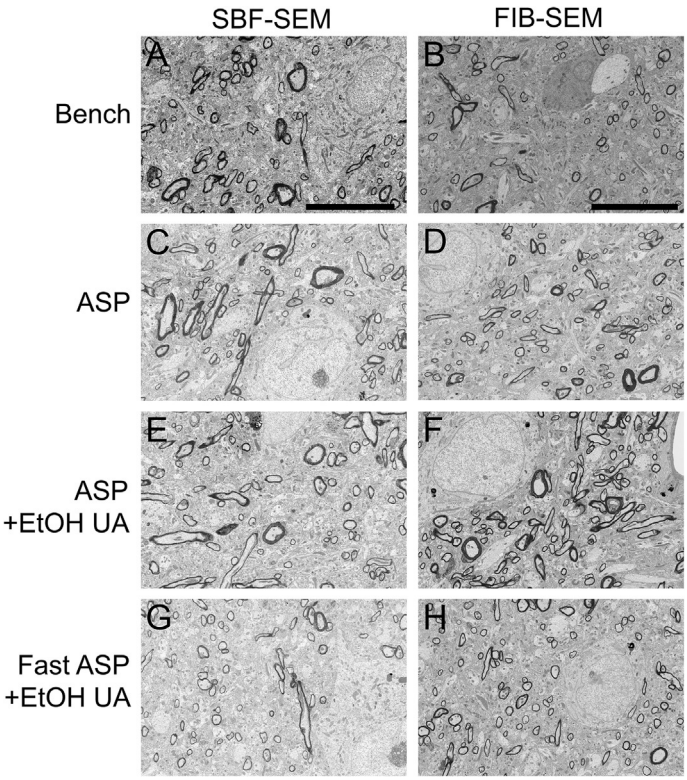

FIG. 4

Contrast comparison for marmoset brain samples between the bench (A, B), ASP-2000 (ASP) (C, D), ASP-2000 with ethanolic UA (ASP+EtOH UA) (E, F), and faster ASP-2000 with ethanolic UA (fast ASP + EtOH UA) (G, H) protocols. Samples were imaged either with SBF-SEM (A, C, E, G) or FIB-SEM (B, D, F, G). Samples were imaged during the same imaging session with the same brightness and contrast. Scale bar = 10 μm.

samples studied by the SBF-SEM (Fig. 5G), indicating that the reduction in incubation times is detrimental to the quality of the sample. Furthermore, as expected, we observed that the lack of staining in the sample decreased the sample conductivity to the extent that imaging during focusing and astigmatism correction, which is usually done at higher magnifications, became difficult due to sample charging.

3.3 Data analysis

3.3.1 Qualitative sample quality comparison

Few differences with respect to image quality could be noted between the bench protocol and ASP-2000 protocols for marmoset brain samples described here. Nuclei, mitochondria, and myelin preservation and staining appear similar across

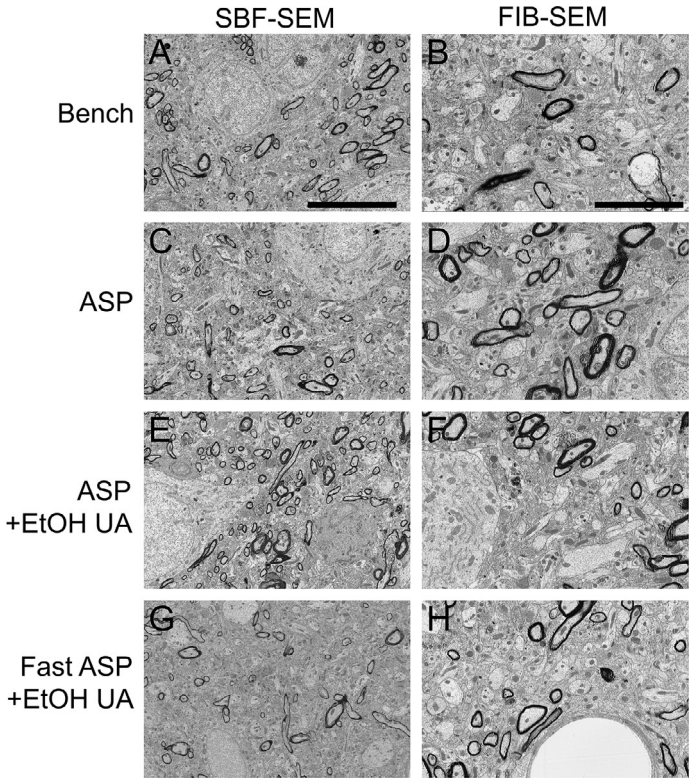

FIG. 5

Ultrastructure comparison for marmoset brain samples between the bench (A, B), ASP-2000 (ASP) (C, D), ASP-2000 with ethanolic UA (ASP+EtOH UA) (E, F), and faster ASP-2000 with ethanolic UA (fast ASP + EtOH UA) (G, H) protocols. Samples were imaged either with SBF-SEM (A, C, D, G) or FIB-SEM (B, D, F, H). Samples were imaged concurrently with optimized contrast for each sample. Scale bar = 10 μm for (A, C, E, G) and scale bar = 5 μm for (B, D, F, H).

all protocols and imaging modalities (Fig. 5A–F, H) with the exception of the fast ASP-2000 protocol for the SBF-SEM as mentioned previously (Fig. 5G). Interestingly, the ASP-2000 protocols increased visualization of the unmyelinated neuronal membranes, with the addition of ethanolic UA allowing for the greatest enhancement of membrane staining. Our results suggest that the ASP-2000 protocol with ethanolic UA (Fig. 5E and F) enhances membrane visualization compared to ASP-2000 protocol with aqueous UA (Fig. 5C and D). It is possible that this increase in membrane visualization may be due to a decrease in overall cytosolic staining, most noted in the regions around nuclei.

Since the use of AT has increased in many imaging facilities, we utilized one of the samples processed with the ASP-2000 for this imaging technique. The Thermo

Scientific Maps™ software for AT was able to automatically identify each section in a ribbon created from the brain sample processed using the ASP-2000 ethanolic UA protocol (Fig. 6). After the ribbons were identified, the next step in the AT workflow was to define the region of interest (ROI) where images will be acquired on each ribbon at the final resolution desired by the operator. Once the ROI was defined, the software accurately found the same area on each ribbon and acquired the images for each plastic section in an automated fashion. Sections 80 nm thick provided adequate signal and contrast to resolve fine ultrastructural detail, such as unmyelinated membranes (Fig. 7). The use of the CBS detector on a FIB-SEM at a working distance of 4 mm allowed for a better image quality and a better lateral resolution compared to SBF-SEM.

Electron microscopy facilities receive a wide variety of samples, and because of this, we aimed to use the ASP-2000 on a tissue to determine stain penetration in a sample that is 1 mm^3. We used tumor tissue from a mouse model of breast cancer. Tumors in general contain a variety of cell types and a variety of tissue densities, which is useful for understanding how protocols stain different cell types and also how stains penetrate tissue.

For mouse tumor tissue, our results indicated that the protocols described here resulted in consistent staining throughout the 1 mm^3 tissue as analyzed by SBF-SEM. Images were acquired in different areas of the tissue processed with the ASP-2000 protocols to confirm that a homogeneous staining was obtained as shown in Fig. 8A, C, E and G. Moreover, the ASP-2000 protocol performed similarly to the bench protocol when imaged with the SBF-SEM (Fig. 8A, A′, C, C′). Importantly, we did not observe any noticeable differences in the staining quality of the cellular components of the tissue when comparing protocols. However, a decrease in contrast was noted by FIB-SEM imaging (Fig. 8B and D).

Similar to the results described previously for the brain tissue, the results obtained with the mouse tissue also indicate that use of ethanolic UA instead of aqueous UA in our protocols resulted in decreased cytosolic contrast but visualization of cell membranes was enhanced, particularly where cells abut one another (Fig. 8E–H). This characteristic was observed when analyzing the samples by both imaging platforms. For the mouse tissue, the faster protocol again resulted in decreased conductivity that caused increased sample charging and drift while focusing and correcting astigmatism (Fig. 8G and H).

3.4 Deep learning-based image quality assessment

For our image analysis, we used noise measurements on blank resin as a way to understand image quality, as noise may disrupt the ability of machine learning algorithms that are frequently utilized in our community to segment cellular features (Fig. 9A). We additionally compared our noise measurements to other selected image quality metrics.

Our results indicate that, for the metrics we selected, patterns emerged dependent on sample type. For brain samples in both the SBF-SEM and FIB-SEM images

FIG. 6

Marmoset brain tissue processed with the ASP-2000 ethanolic UA protocol visualized in the Thermo Scientific Maps™ array tomography workflow. The software automatically localized each individual section and the user later defined the specific region of interest for the image acquisition. Scale bar = 1 mm.

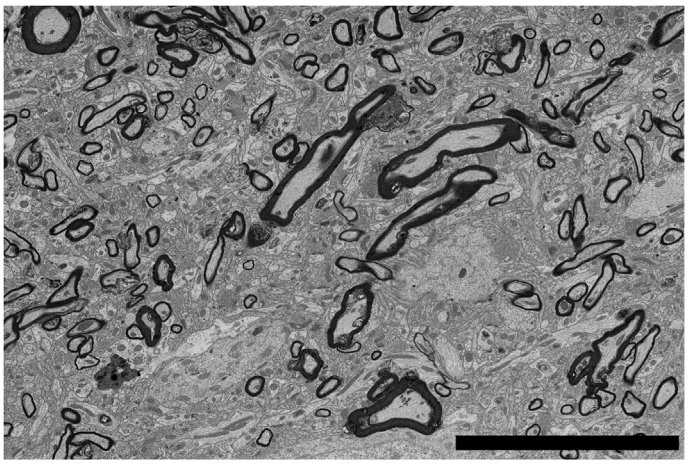

FIG. 7

Marmoset brain tissue processed with the ASP-2000 ethanolic UA protocol was imaged using an array tomography workflow. Scale bar = 10 μm.

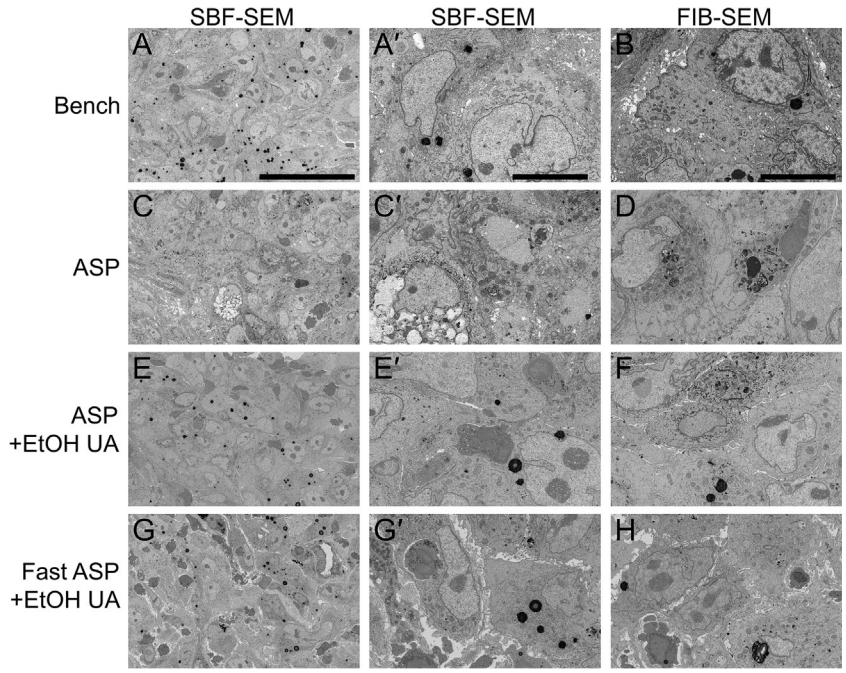

FIG. 8

Ultrastructure and contrast comparison for mouse tumor samples between the bench (A, A′, B), ASP-2000 (ASP) (C, C′, D), ASP-2000 with ethanolic UA (ASP+EtOH UA) (E, E′, F), and faster ASP-2000 with ethanolic UA (fast ASP + EtOH UA) (G, G′, H) protocols. SBF-SEM images: A, A′, C, C′, E, E′, G, G′, and FIB-SEM images: B, D, F, H. Scale bar = 50 μm for (A, C, E, G) and scale bar = 10 μm for (A′, B, C′, D, E′, F, G′, H).

analyzed, the ASP-2000 protocol with ethanolic UA resulted in similar and occasionally better image quality scores when compared to the other protocols tested (Fig. 9A–H). For tumor samples, the bench protocol tended to have the best image quality scores, followed by the ASP-2000 protocol, the ASP-2000 protocol with ethanolic UA, and finally the fast ASP-2000 protocol (Fig. 9A–H).

The metric that was the most straightforward and reliable in our analysis was the standard deviation in the hand-annotated resin areas, as we are sure it only considers noise and not signal (Fig. 9A). SSIM and SRSIM have very small variations, which could mean they are not suited for the task, but they are correlated with most other metrics (Fig. 9C and D).

For further analysis, we created Pearson and Spearman correlation matrices between the metrics analyzed (Fig. 9). The standard deviation in resin is the closest that we have to a ground truth evaluation of the noise. This result strongly correlated to DISTS, SRSIM and SSIM, indicating that these metrics are good evaluators of the noise in our images. On the other hand, BRISQUE and PSNR exhibit a strong correlation but are poorly correlated to the other metrics, which indicates that they use different features to yield their evaluation (Fig. 10).

The annotated resin areas (Fig. 3) were also used to evaluate denoised images we obtained using Noise2Void (Krull et al., 2019) as a way to understand how the processing protocols may perform with machine learning algorithms. After denoising, noise values decreased for all samples, regardless of protocol or imaging modality. Noise was reduced by an order of magnitude for FIB-SEM images and by half to 85% for SBF-SEM images while retaining useful signals. Samples imaged with the FIB-SEM had noise values all within one standard deviation regardless of protocol used or tissue type. Surprisingly, after denoising, samples processed with ASP-2000 protocols had less noise than their bench-processed counterparts (Fig. 11). In conclusion, based on our image analysis results, all of the sample processing protocols described here can be used to efficiently train a deep learning architecture to reduce noise.

4 Discussion

The ASP-2000 automated specimen processor delivers on its promise to decrease the amount of time required for specimen preparation for vEM, without compromising the quality of the specimens and images acquired. Overall, in our hands, the sample preparation time for vEM using this automated processor is reduced to almost a tenth of the time required with conventional bench methods. As shown here, staining and image noise between our ASP-2000 protocols and the bench method are in general comparable, particularly for vEM methods that can tolerate less staining, i.e., FIB-SEM and array tomography. In fact, as suggested by our image quality metrics, some samples such as brain tissues may benefit from a reduction in sample staining. In general, we observed that the substitution of ethanolic UA for aqueous UA in the staining procedure as well as a reduction of overall staining times increases the

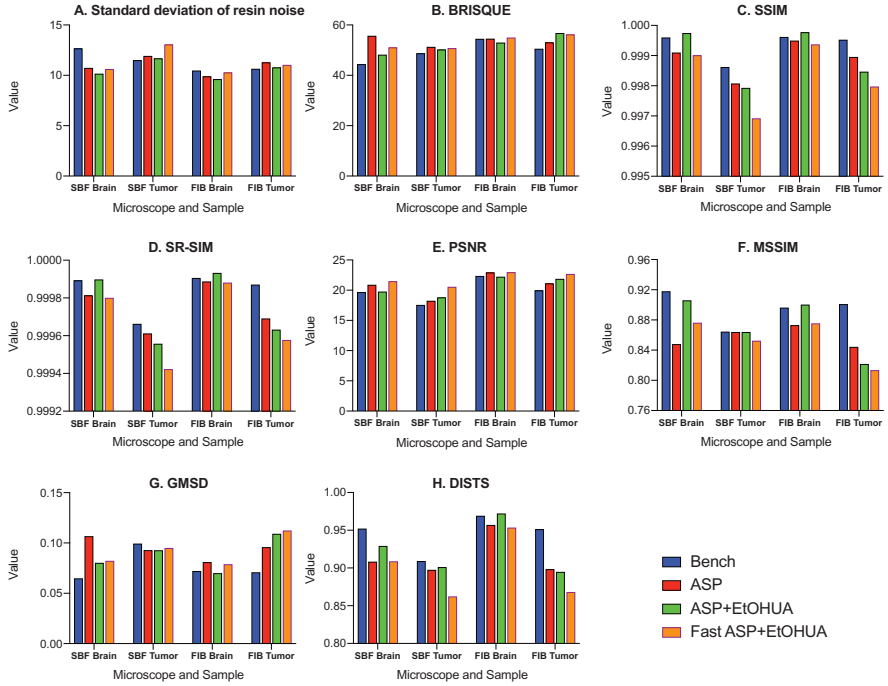

FIG. 9

Image quality metrics for brain and tumor samples imaged with the SBF-SEM (SBF) or FIB-SEM (FIB) imaging platforms processed with the bench, ASP-2000 (ASP) ASP-2000 with ethanolic UA (ASP+EtOHUA) or fast ASP-2000 with ethanolic UA (fast ASP+EtOHUA) protocols. The following metrics were evaluated and compared to the standard deviation of noise on resin (A), (B) Blind/Referenceless Image Spatial Quality Evaluator (BRISQUE), (C) Structural Similarity Index Measure (SSIM), (D) Spectral Residual Based Similarity Index Measure (SR-SIM), (E) Peak Signal-to-Noise Ratio (PSNR), (F) Multi-scale Structural Similarity Index Measure (MSSIM), (G) Gradient Magnitude Similarity Deviation (GMSD), and (H) Deep Image Structure and Texture Similarity (DISTS).

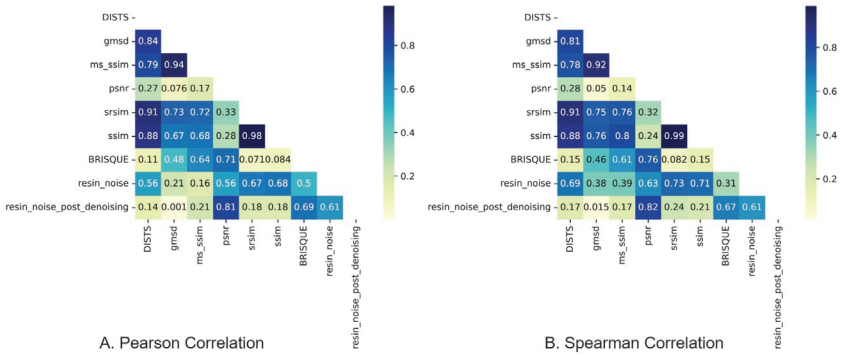

FIG. 10

Pearson (A) and Spearman (B) correlation analyses between image analysis metrics. The following metrics were compared: the standard deviation of noise on resin (resin_noise), Blind/Referenceless Image Spatial Quality Evaluator (BRISQUE), Structural Similarity Index Measure (ssim), Spectral Residual Based Similarity Index Measure (srsim), Peak Signal-to-Noise Ratio (psnr), Multi-scale Structural Similarity Index Measure (ms_sim), Gradient Magnitude Similarity Deviation (gmsd), and Deep Image Structure and Texture Similarity (DISTS).

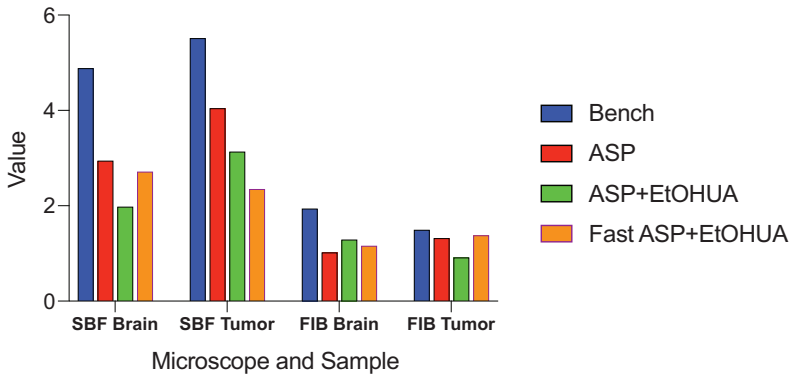

FIG. 11

Results of image denoising for brain and tumor samples imaged on the SBF-SEM (SBF) and FIB-SEM (FIB) imaging platforms processed with the bench, ASP-2000 (ASP) ASP-2000 with ethanolic UA (ASP+EtOHUA) or fast ASP-2000 with ethanolic UA (fast ASP+EtOHUA) protocols.

contrast between membranes and cytosol. Our results track well with work performed by Thomas et al. (2021) wherein the researchers optimized the bench protocol established by Hua et al. (2015) by reducing staining times and including ethanolic acid for 80 μm thick ferret brain sections.

The ASP-2000 protocol we have described here is the fastest protocol we can perform for adequate staining of samples processed for SBF-SEM and/or FIB-SEM. However, based on our results, longer staining times may contribute to increased conductivity of the specimen to allow for better performance for SBF-SEM. With the use of the ASP-2000, adjustment staining times for protocol optimization is very simple via modifications of stored methods in the user interface. This can be achieved simply by increasing the number of repetitions performed at each staining step. Different protocols can be stored on the user interface and can be modified and saved for further optimizations.

Another of the advantages of automating the sample preparation procedure is that in general, any modification in the protocol does not necessarily require longer days from the operator, as may be required from conventional bench protocols. In the bench protocol used here, overall contrast is additionally enhanced by heating the samples in UA to 50 °C (Hua et al., 2015). This could also be applied to the ASP-2000 protocol by switching out the TCH plate with UA during the second osmium tetroxide staining.

Automated specimen processing also ensures samples are reproducible. In the 12-column plates, all the samples are exposed to the same batches of reagents for the same amount of time. With an automated system, there is no need to worry about staining changes due to being called away from the bench during a protocol. Furthermore, comparisons between different stains during a screening or optimization procedure can be easily accomplished in a 96-well plate, where each well could conceivably hold a different stain or concentration.

Microwave methods may stain samples in the same amount of time as the ASP-2000. However, microwaves require an operator to stay by the microwave unless times are particularly long between sample preparation steps. Because the ASP-2000 can move the sample through staining and rinsing steps, technician time is freed to perform other duties.

Reducing active operator time performing protocols not only frees up technician time, but also reduces the overall cost for the researcher requiring vEM studies in a university resource core or EM facility. For vEM bench processing in our facility, consumables make up about 6% of the cost of processing a sample, with technician time making up the rest of the cost. Automated protocols have reduced processing costs in our laboratory by half. Having less expensive sample processing costs will help investigators to optimize the use of their funds by dedicating them to the imaging cost, which will result in more data. Moreover, the ASP-2000 requires less volume of all the solutions needed as compared to bench-top methods, which also reduces the total cost of the sample preparation process.

As with any technique, the ASP-2000 is not without limitations. The pipettor only allows for up to eight samples to be processed at once, which may not be adequate in laboratories requiring high throughput sample preparation, like clinics or pathology laboratories. Two capsules could possibly be added in series to each other so that up to 16 samples could be processed at once; however, we have not tried this as the eight sample capacity has been adequate for our research needs. The use of the mPrep/s™

capsules requires that only tissue and tissue-like samples can be processed. Samples such as cells grown on coverslips are too large for this machine. Cellular pellets could be enrobed in agarose, but the higher temperatures used for TCH and lead staining melt the low melting point agarose typically used, leading to a loss of sample and possibly clogging the capsule holes. However, cellular pellets that have undergone high pressure freezing and freeze substitution may be robust enough to be stained, dehydrated, and embedded in resin with the ASP-2000. We have previously noted that the decrease in staining time results in decreased sample conductivity, which can lead to an increase in sample charging during imaging, though this can be ameliorated by programming more repetitions to increase staining times. Conductivity issues can be partially compensated for by imaging the samples at low vacuum, though this could potentially compromise the image quality. Furthermore, conductivity issues on SBF-SEMs can also be ameliorated by focal charge compensation available on some SBF-SEM models (Deerinck et al., 2018; Unger, Neujahr, Hawes, & Hummel, 2020). We have observed that vibratome sections thinner than 100 μm tend to dry out during the processing described here, resulting in samples with poor staining quality (data not shown). The use of this equipment creates more contaminated plastic waste than conventional bench top methods, which needs to be disposed following specific regulations at each institution.

In conclusion, our results indicate that the ASP-2000 automated specimen processor allows for adequate staining of samples and the resulting image quality is suitable for deep learning-based models, such as those used for automated segmentation. This automated processor is capable of being programmed for a variety of samples and protocol needs. Moreover, its utilization decreases the overall time and cost for sample processing, decreases the operator time required, and improves protocol reproducibility. Importantly, technicians performing the ASP-2000 methods described here only interact with hazardous chemicals during the setup and cleanup steps of the protocols, reducing safety concerns (see section "Key resources table").

Key resources table

Reagent or Resource	Source	Identifier
Biological Samples		
Marmoset brain	Salk Institute for Biological Studies	
Mouse-derived syngeneic transplants	Oregon Health and Science University	
Chemicals, Peptides, and Recombinant Proteins		
16% formaldehyde, aqueous	Electron Microscopy Sciences	15714
25% glutaraldehyde, aqueous	Electron Microscopy Sciences	16120

—cont'd

Reagent or Resource	Source	Identifier
Sodium cacodylate	Electron Microscopy Sciences	12300
4% osmium tetroxide, aqueous	Ted Pella	18463
Potassium ferricyanide	Sigma Aldrich	702587
Thiocarbohydrazide	Sigma Aldrich	223220
Uranyl acetate	Electron Microscopy Sciences	22400
Lead nitrate	Electron Microscopy Sciences	17900
Aspartic acid	Sigma-Aldrich	11195
Acetone	Electron Microscopy Sciences	10014
Embed812 resin kit	Electron Microscopy Sciences	14121
Leitsilber	Ted Pella	16035
H20E EPO-TEK silver conductive epoxy	Ted Pella	16014
Rubber cement	Staples	473595
Xylene	Sigma-Aldrich	534056
Software and Algorithms		
ASP software	Microscopy Innovations	4.18f
Maps	Thermo Scientific	3.13 or 3.9
Maps with array tomography plugin	Thermo Scientific	3.21
Other		
mPrep™ ASP-2000™ automatic specimen processor	Microscopy Innovations	41120
mPrep/s™ capsules without screens	Microscopy Innovations	22550
mPrep/s™ capsules with screens	Microscopy Innovations	22505
mPrep/Bench™ silicone rack	Microscopy Innovations	34000
96-well plates	Microscopy Innovations	51011
12-channel reagent reservoir	Microscopy Innovations	52502
Pierce heat-seal foil plate sheets	Microscopy Innovations	53070
SEM pin stub for Volumescope II	Ted Pella	16145
SEM pin stub	Ted Pella	16111
Transfer pipets	Fisher Scientific	13-711-7M
Centrifuge tubes	Fisher Scientific	14-222-180
Flat embedding mold	Ted Pella	10504
Carbon conductive tabs	Ted Pella	16084-15
Silicon chip specimen supports, 20×20 mm	Ted Pella	16004

Acknowledgments

This research was funded by the OHSU Center for Spatial Systems Biomedicine at Oregon Health and Science University, NIH-NCI Cancer Center Support Grant 2P30CA069533 and OHSU Faculty Initiative Pool Award to CSL. Processing and imaging were performed at the Multiscale Microscopy Core Facility, a University Shared Resource at OHSU. Special thanks to Gordon Mills and Dong Zhang at the OHSU Knight Cancer Institute for providing mouse tissue and Casey Vanderlip and Courtney Glavis-Bloom at Salk Institute for Biological Studies for providing marmoset brain tissue. We also acknowledge support from the M. J. Murdock Charitable Trust for providing funds to purchase the Thermo Scientific Helios 5 UC FIB-SEM.

References

Benson, E., Kidd, G., Campbell, J., & Goodman, S. (2020). Serial block-face SEM of brain tissue using rapid automated preparation. *Microscopy and Microanalysis*, *26*(S2), 1372–1373.

Chow, L. S., & Paramesran, R. (2016). Review of medical image quality assessment. *Biomedical Signal Processing and Control*, *27*, 145–154. https://doi.org/10.1016/j.bspc.2016.02.006.

Deerinck, T. J., Bushong, E. A., Thor, A., & Ellisman, M. H. (2010). NCMIR methods for 3D EM: A new protocol for preparation of biological specimens for serial block face scanning electron microscopy. *Microscopy*, *1*, 6–8.

Deerinck, T. J., Shone, T. M., Bushong, E. A., Ramachandra, R., Peltier, S. T., & Ellisman, M. H. (2018). High-performance serial block-face SEM of nonconductive biological samples enabled by focal gas injection-based charge compensation. *Journal of Microscopy*, *270*(2), 142–149. https://doi.org/10.1111/jmi.12667.

Ding, K., Ma, K., Wang, S., & Simoncelli, E. P. (2020). Image quality assessment: Unifying structure and texture similarity. *IEEE Transactions on Pattern Analysis and Machine Intelligence*, *44*(5), 2567–2581.

Goodman, S. L., Campbell, J. M., Wu, K., Chan, H., Bouchet-Marquis, C., Braun, R. K., et al. (2019). Effects of postnatal Hyperoxia exposure on cardiac muscle examined with 3D serial block face SEM using rapid automated sample preparation. In *Paper presented at the microscopy and microanalysis conference*.

Guérin, C. J., Kremer, A., Borghgraef, P., & Lippens, S. (2019). Targeted studies using serial block face and focused ion beam scan electron microscopy. *Journal of Visualized Experiments*, (150), e59480. https://doi.org/10.3791/59480.

Guérin, C. J., Kremer, A., Borghgraef, P., Shih, A. Y., & Lippens, S. (2019). Combining serial block face and focused ion beam scanning electron microscopy for 3D studies of rare events. In *Vol. 152. Methods in cell biology* (pp. 87–101). Elsevier.

Hore, A., & Ziou, D. (2010). Image quality metrics: PSNR vs. SSIM. In *Paper presented at the 2010 20th international conference on pattern recognition*.

Hua, Y., Laserstein, P., & Helmstaedter, M. (2015). Large-volume en-bloc staining for electron microscopy-based connectomics. *Nature Communications*, *6*, 7923. https://doi.org/10.1038/ncomms8923.

Ishibashi, M., Keung, J., Morgans, C. W., Aicher, S. A., Carroll, J. R., Singer, J. H., et al. (2022). Analysis of rod/cone gap junctions from the reconstruction of mouse photoreceptor terminals. *eLife*, *11*, e73039. Retrieved from https://www.ncbi.nlm.nih.gov/pmc/articles/PMC9170248/pdf/elife-73039.pdf.

Johnson, B. E., Creason, A. L., Stommel, J. M., Keck, J. M., Parmar, S., Betts, C. B., et al. (2022). An omic and multidimensional spatial atlas from serial biopsies of an evolving metastatic breast cancer. *Cell Reports Medicine*, *3*(2), 100525. https://doi.org/10.1016/j.xcrm.2022.100525.

Kizilyaprak, C., Stierhof, Y. D., & Humbel, B. M. (2019). Volume microscopy in biology: FIB-SEM tomography. *Tissue & Cell*, *57*, 123–128. https://doi.org/10.1016/j.tice.2018.09.006.

Kremer, A., Lippens, S., Bartunkova, S., Asselbergh, B., Blanpain, C., Fendrych, M., et al. (2015). Developing 3D SEM in a broad biological context. *Journal of Microscopy*, *259*(2), 80–96. https://doi.org/10.1111/jmi.12211.

Krull, A., Buchholz, T.-O., & Jug, F. (2019). Noise2void-learning denoising from single noisy images. In *Paper presented at the Proceedings of the IEEE/CVF conference on computer vision and pattern recognition*.

Lippens, S., Kremer, A., Borghgraef, P., & Guérin, C. J. (2019). Chapter 4: Serial block face-scanning electron microscopy for volume electron microscopy. In T. Müller-Reichert, & G. Pigino (Eds.), *Vol. 152. Methods in cell biology* (pp. 69–85). Academic Press.

Lopez, C. S., Riesterer, J., Loftis, K., Kwon, S., Thibault, G., Williams, M., et al. (2018). Correlative light and 3D electron microscopy of subnuclear structures. *Microscopy and Microanalysis*, *24*(S1), 1222–1223.

McClain, M., Harwood, M., & Nowotarski, S. (2019). Automated heavy metal tissue staining for serial block face imaging with the ASP-1000. In *Paper presented at the Microscopy and Microanalysis Conference*.

McClain, M., Nowotarski, S. H., Zhao, X., & Alvarado, A. S. (2017). *Rapid automated en bloc staining for SEM of sections*. (Paper presented at the Microscopy and Microanalysis Conference).

Midgett, M., López, C. S., David, L., Maloyan, A., & Rugonyi, S. (2017). Increased hemodynamic load in early embryonic stages alters myofibril and mitochondrial organization in the myocardium. *Frontiers in Physiology*, *8*, 631. Retrieved from https://www.ncbi.nlm.nih.gov/pmc/articles/PMC5582297/pdf/fphys-08-00631.pdf.

Mikula, S., Binding, J., & Denk, W. (2012). Staining and embedding the whole mouse brain for electron microscopy. *Nature Methods*, *9*(12), 1198–1201. https://doi.org/10.1038/nmeth.2213.

Mikula, S., & Denk, W. (2015). High-resolution whole-brain staining for electron microscopic circuit reconstruction. *Nature Methods*, *12*(6), 541–546. https://doi.org/10.1038/nmeth.3361.

Mittal, A., Moorthy, A. K., & Bovik, A. C. (2012). No-reference image quality assessment in the spatial domain. *IEEE Transactions on Image Processing*, *21*(12), 4695–4708. https://doi.org/10.1109/TIP.2012.2214050.

Peddie, C. J., & Collinson, L. M. (2014). Exploring the third dimension: Volume electron microscopy comes of age. *Micron*, *61*, 9–19. https://doi.org/10.1016/j.micron.2014.01.009.

Peddie, C. J., Genoud, C., Kreshuk, A., Meechan, K., Micheva, K. D., Narayan, K., et al. (2022). Volume electron microscopy. *Nature Reviews Methods Primers*, *2*(1). https://doi.org/10.1038/s43586-022-00131-9.

Peloggia, J., Munch, D., Meneses-Giles, P., Romero-Carvajal, A., Lush, M. E., Lawson, N. D., et al. (2021). Adaptive cell invasion maintains lateral line organ homeostasis in response to environmental changes. *Developmental Cell*, *56*(9), 1296–1312. e1297 https://doi.org/10.1016/j.devcel.2021.03.027.

Riesterer, J. L., Lopez, C. S., Stempinski, E. S., Williams, M., Loftis, K., Stoltz, K., et al. (2020). A workflow for visualizing human cancer biopsies using large-format electron microscopy. *Methods in Cell Biology*, *158*, 163–181. https://doi.org/10.1016/bs.mcb.2020.01.005.

Rykiel, G., Lopez, C. S., Riesterer, J. L., Fries, I., Deosthali, S., Courchaine, K., et al. (2020). Multiscale cardiac imaging spanning the whole heart and its internal cellular architecture in a small animal model. *eLife*, *9*, e58138. https://doi.org/10.7554/eLife.58138.

Schieber, N. L., Machado, P., Markert, S. M., Stigloher, C., Schwab, Y., & Steyer, A. M. (2017). Chapter 4: Minimal resin embedding of multicellular specimens for targeted FIB-SEM imaging. In T. Müller-Reichert, & P. Verkade (Eds.), *Vol. 140. Methods in cell biology* (pp. 69–83). Academic Press.

Tapia, J. C., Kasthuri, N., Hayworth, K. J., Schalek, R., Lichtman, J. W., Smith, S. J., et al. (2012). High-contrast en bloc staining of neuronal tissue for field emission scanning electron microscopy. *Nature Protocols*, *7*(2), 193–206. https://doi.org/10.1038/nprot.2011.439.

Thomas, C. I., Ryan, M. A., Scholl, B., Guerrero-Given, D., Fitzpatrick, D., & Kamasawa, N. (2021). Targeting functionally characterized synaptic architecture using inherent fiducials and 3D correlative microscopy. *Microscopy and Microanalysis*, *27*(1), 156–169. https://doi.org/10.1017/S1431927620024757.

Unger, A.-K., Neujahr, R., Hawes, C., & Hummel, E. (2020). Improving serial block face SEM by focal charge compensation. In I. Wacker, E. Hummel, S. Burgold, & R. Schröder (Eds.), *Volume Microscopy* (pp. 165–178). New York, NY: Springer US.

Wacker, I., & Schroeder, R. R. (2013). Array tomography. *Journal of Microscopy*, *252*(2), 93–99. https://doi.org/10.1111/jmi.12087.

Wang, Z., Bovik, A. C., Sheikh, H. R., & Simoncelli, E. P. (2004). Image quality assessment: From error visibility to structural similarity. *IEEE Transactions on Image Processing*, *13*(4), 600–612. https://doi.org/10.1109/tip.2003.819861.

Wang, Z., Simoncelli, E. P., & Bovik, A. C. (2003). Multiscale structural similarity for image quality assessment. In *Paper presented at the The Thrity-Seventh Asilomar Conference on Signals, Systems & Computers, 2003*.

Xue, W., Zhang, L., Mou, X., & Bovik, A. C. (2013). Gradient magnitude similarity deviation: A highly efficient perceptual image quality index. *IEEE Transactions on Image Processing*, *23*(2), 684–695.

Zhang, L., & Li, H. (2012). SR-SIM: A fast and high performance IQA index based on spectral residual. In *Paper presented at the 2012 19th IEEE international conference on image processing*.